Immobilization of streptavidin on 4H–SiC for biosensor development

Elissa H. Williams [a,b,c,*], Albert V. Davydov [b], Abhishek Motayed [b], Siddarth G. Sundaresan [b,d],
Peter Bocchini [b,e], Lee J. Richter [b], Gheorghe Stan [b], Kristen Steffens [b], Rebecca Zangmeister [b],
John A. Schreifels [a], Mulpuri V. Rao [c]

[a] Department of Chemistry and Biochemistry, George Mason University, Fairfax, VA 22030, USA
[b] Material Measurement Laboratory, NIST, Gaithersburg, MD 20899, USA
[c] Department of Electrical and Computer Engineering, George Mason University, Fairfax, VA 22030, USA
[d] GeneSiC Semiconductor Inc., Dulles, VA 20166, USA
[e] Department of Mechanical Engineering, University of Delaware, Newark, DE 19716, USA

ARTICLE INFO

ABSTRACT

A sequential layer formation chemistry is demonstrated for the functionalization of silicon carbide (SiC) appropriate to biosensing applications. (0 0 0 1) 4H–SiC was functionalized with 3-aminopropyltriethoxysilane (APTES) and subsequently biotinylated for the selective immobilization of streptavidin. Atomic force microscopy, X-ray photoelectron spectroscopy, ellipsometry, fluorescence microscopy, and contact angle measurements were utilized to determine the structure, thickness, wettability, and reactivity of the resulting surface after each functionalization step. Optimization of the APTES layer was found to be critical to the success of the subsequent steps; multilayer, polymeric films resulted in irreproducible behavior. It was shown that there was significant non-specific (electrostatic) binding of streptavidin to APTES functionalized SiC, thus revealing the importance of a uniform biotinylation step prior to streptavidin attachment. The experimental results demonstrate that the APTES functionalized and biotinylated SiC surface has the potential to be employed as a biosensing platform for the selective detection of streptavidin molecules.

© 2012 Elsevier B.V. All rights reserved.

1. Introduction

Over the past few years, there has been an increased interest in the fabrication of semiconductor biosensors that have the ability to electrically detect adsorbed biomolecules with great selectivity and sensitivity [1–5]. The efficiency of such sensors is enabled by chemi-resistive transduction mechanisms, where the change in surface potential due to selective molecular absorption affects the device conductance [6]. Of the readily available semiconductor materials, SiC is an attractive substrate for biosensing applications due to its unique electronic properties, mechanical robustness, chemical inertness, thermal stability, non-toxicity, and biocompatibility [7–11]. In order to enable SiC-based devices that utilize direct, electronic sensing of biomolecules, one must first develop an analyte-specific functionalization of SiC and deduce mechanisms by which the functional and analyte molecules bind to the SiC surface. Numerous conjugation techniques have been developed for the attachment of specific biomolecules to surfaces through the use of various linking molecules [12,13]. The covalent attachment of APTES on oxidized surfaces is widely used as the first step of surface functionalization for the optical and electrical detection of proteins and DNA [1,3,14–16]. APTES functionalized semiconductor surfaces result in great versatility and adaptability since amine groups can react with any biomolecule containing or modified with an ester group to form a stable amide bond. To date, only one research group, Yakimova et al. [7], has studied the immobilization of APTES on SiC surfaces. Yakimova et al. reported the successful covalent attachment of APTES to (0 0 0 1) 4H–SiC using a vapor phase deposition.

The biotin–streptavidin system, in which four biotin molecules bind to one streptavidin molecule, is one of the most stable and selective noncovalent biological binding couples known and hence it is often employed as a model system to study bio-recognition events [15,16]. Additionally, the multi-functionality of streptavidin makes it a useful coupling agent for nano-engineering applications [17,18]. A commercially available sulfonated and esterified form of biotin (sulfo-NHS-biotin) enables simple and efficient

biotin labeling of any primary amine containing molecule [3]. Thus, biotinylation of an APTES functionalized SiC surface and subsequent streptavidin immobilization is achievable and presents a protein–ligand interaction that is ideal for the development of a biosensor [19].

This paper presents results of the first detailed and comprehensive study of APTES attachment to the (0 0 0 1) Si-face of 4H–SiC. AFM, XPS, ellipsometry, and contact angle measurements were utilized to determine the optimum surface conditions for the covalent attachment of APTES. The effects of APTES deposition duration on the structure, thickness, reactivity, and wettability of the resulting APTES layer on SiC were investigated. The immobilization of biotin and streptavidin on the APTES functionalized SiC surface and the effect of APTES deposition conditions on the attachment of biotin and streptavidin were studied. Selective streptavidin immobilization on biotinylated SiC was monitored using fluorescence microscopy. In addition, the non-specific binding of streptavidin as well as BSA to bare, APTES functionalized, and biotinylated SiC surfaces was examined experimentally.

2. Material and methods

Silane functionalization, biotinylation, and streptavidin immobilization were performed on SiC substrates using Scheme 1. A commercial 76.2 mm (3 in.) diameter wafer of (n-doped) 4H–SiC (0 0 0 1)[1] was cut into 5 mm × 5 mm squares. The samples were immersed for 5 min in trichloroethylene, followed by acetone, and then in isopropanol. They were further cleaned using a standard RCA cleaning procedure [20].

To improve the reactivity of the SiC surface and to remove any remaining organic contaminants, the SiC samples were treated in an oxygen plasma [21] (Fischione Instruments, Model 1020 Plasma Cleaner[2]) in a 20% oxygen/80% argon gas mixture for 1 min. Oxygen plasma treatment grows a thin oxide that facilitates the creation of surface silanol groups (see step A in Scheme 1) which are necessary for APTES condensation on the SiC surface [22]. The SiC samples were exposed to air for 2–3 h following oxygen plasma cleaning to ensure surface chemisorption of water molecules. It has been proposed that APTES hydrolysis can occur most efficiently if there is sufficient surface water available for the reaction [23]. The moist silanol-terminated SiC samples were immersed in a 1:49 volume fraction (v/v) solution of APTES (99% APTES, Sigma–Aldrich) in toluene (99.8% anhydrous, Sigma–Aldrich) for a duration of 5 min, 1 h, or 16 h followed by ultrasonication to minimize the non-specific attachment of APTES to the SiC surface. A glove bag with a nitrogen environment at room temperature was utilized for APTES attachment. Following the controlled deposition of APTES (see Scheme 1, step B) on the SiC surface, the samples were ultrasonicated for 10 min in toluene and for 1 min in isopropanol (99% anhydrous, Oriole Brand, Warner–Graham Co.) to remove any loosely adsorbed APTES molecules [22]. The functionalized SiC samples were dried under a stream of nitrogen gas. Biotinylation of the SiC surface (see Scheme 1, step C) was achieved by placing the APTES functionalized samples in a 5 mg/mL solution of sulfo-NHS-biotin (sulfo-*N*-hydroxysuccinimide biotin ester sodium salt, Thermo Scientific) in 0.01 M phosphate buffer (pH = 7.4, Sigma–Aldrich) for 2 h at room temperature. The terminal amino

group of the APTES functionalized samples reacts with the ester linkage in sulfo-NHS-biotin thus leading to the formation of a stable amide bond and a biotinylated surface. The biotinylated SiC samples were ultrasonicated in phosphate buffer for 15 min to remove physisorbed biotin molecules, rinsed with deionized water, and dried with a stream of nitrogen gas [15]. Streptavidin immobilization on the biotinylated surface (Scheme 1, step D) was achieved by exposing the samples to a 0.058 mg/mL solution of streptavidin-cy3 conjugate protein (1 mg/mL, pH 7.4, Sigma–Aldrich) in 0.01 M phosphate buffer (pH = 7.4, Sigma–Aldrich) containing 0.05% Tween20 (polyethylene glycol sorbitan monolaurate, Sigma–Aldrich) for 2 h at room temperature. A 2 h protein exposure time is typical for functionalization protocols described in the literature [3,4,15], and was thus utilized in the present study. However, it is important to point out that since biotin–streptavidin binding occurs on the second time-scale, a much shorter exposure time can be used in device sensing experiments [3]. Tween20 was used to minimize non-specific binding of streptavidin to the biotinylated SiC surface. After the immobilization of streptavidin, the samples were rinsed in a phosphate buffer containing 0.05% Tween20 solution for 15 min to remove loosely adsorbed streptavidin molecules, rinsed in phosphate buffer for 30 s to wash off the Tween20 solution and physisorbed streptavidin molecules, and dried under a stream of nitrogen gas.

The binding of FBS to 5 min APTES functionalized SiC and to biotinylated SiC was studied as follows: 10 mL of 5 mg/mL biotin (in 0.01 M phosphate buffer, pH = 7.4) was mixed with 12 mL of 0.058 mg/mL streptavidin-cy3 (in 0.01 M phosphate buffer, pH = 7.4) and 11 μL of Tween20 resulting in a solution of FBS. This solution was allowed to incubate at room temperature for 10 min. APTES and biotinylated SiC samples were subsequently immersed in the FBS solution for 2 h at room temperature, rinsed in a phosphate buffer containing 0.05% Tween20 solution for 15 min, rinsed in phosphate buffer for 30 s, and dried under a stream of nitrogen gas.

To test the selectivity of biotinylated SiC, the 5 min APTES functionalized and biotinylated samples were immersed in a solution of 0.058 mg/mL FITC labeled BSA (Sigma–Aldrich) in 0.01 M tris buffer (tris(hydroxymethyl)aminomethane, pH = 7.4, Sigma–Aldrich) containing 0.05% Tween20 for 2 h at room temperature. BSA is a serum protein that has no affinity for biotin and thus there should be no conjugation of BSA to the biotinylated SiC samples. Following sample immersion in the BSA solution, the samples were rinsed in a tris buffer containing 0.05% Tween20 solution for 15 min, rinsed in tris buffer for 30 s, and dried under a stream of nitrogen gas.

SiC samples were characterized using ellipsometry, fluorescence microscopy, AFM, XPS, and contact angle measurements.

2.1. Ellipsometry

Optical thickness measurements were performed on the SiC samples with a multichannel, spectroscopic ellipsometer (M2000-DI, J.A. Woollam Co., Inc.) at an incident angle of 70°. A weakly focused, ≈0.3 mm diameter beam was used. To avoid coherent artifacts due to reflection from the back of the double sided polished wafers, only the spectral region from 190 nm to 350 nm, where SiC is absorbing, was included in the analysis. The layer thickness was determined with vendor supplied software using up to five layers (SiC, SiO_2, organic, organic, and protein). The dielectric function for SiC was derived from a multi-angle, multi-sample (freshly etched, plasma treated) analysis. The analysis treated the SiC as isotropic [24] and the results were similar to those in the literature [25]. The dielectric function for SiO_2 was taken from the literature [26]. It was necessary to account for the UV absorption of both the organic (APTES/biotin) and protein layers. A simple model with a single

---

[1] Hereafter, all functionalization steps with the corresponding characterization data are reported for the Si-terminated (0 0 0 1) face of SiC; both Si- and C-terminated faces exhibited practically identical bio-functionalization behavior based on preliminary results.

[2] Commercial equipment and material suppliers are identified in this paper to adequately describe experimental procedures. This does not imply endorsement by NIST.
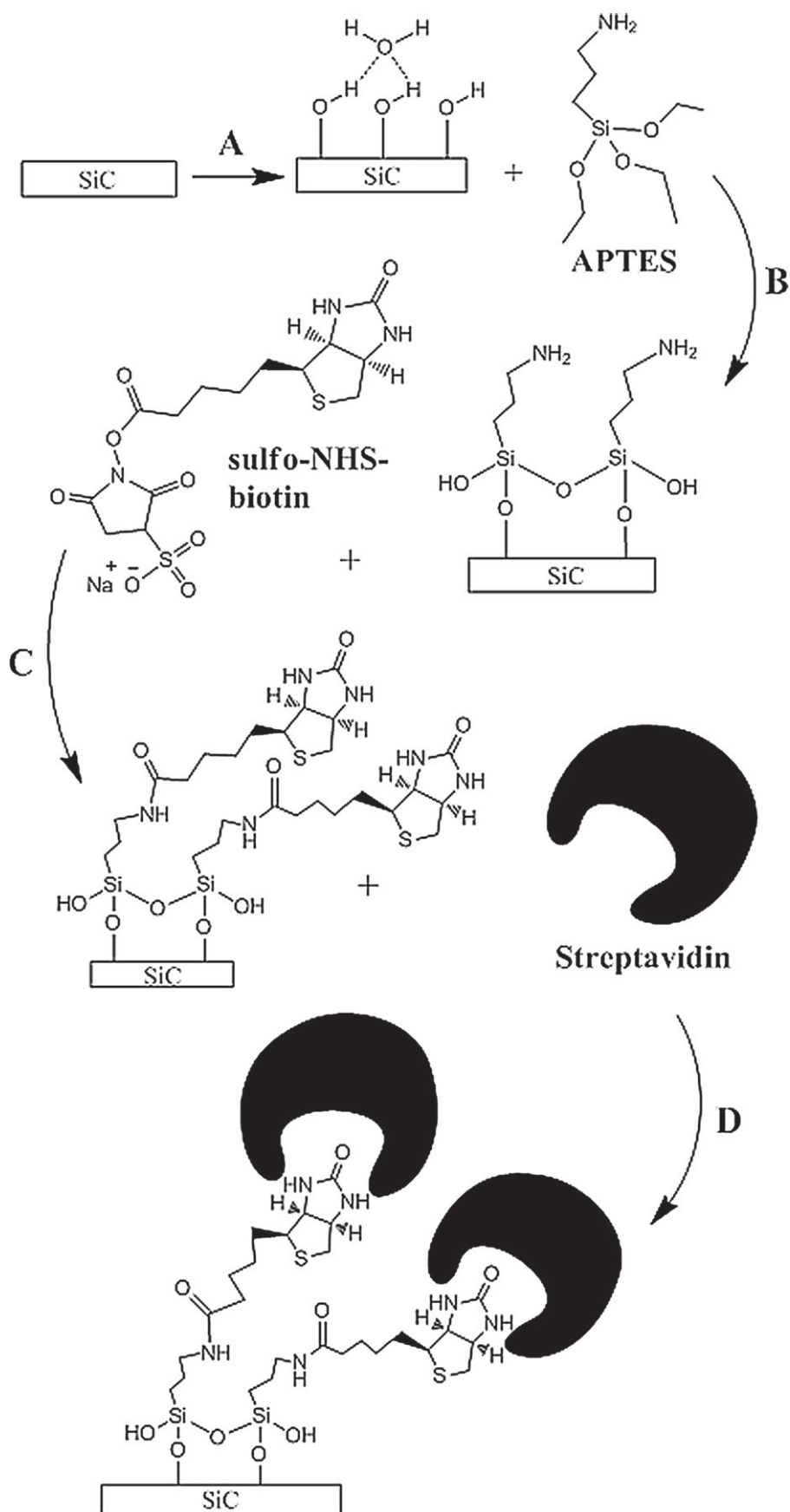
Scheme 1. Functionalization reactions for the attachment of streptavidin to (0 0 0 1) SiC. (A) RCA cleaning, oxygen plasma cleaning, and adsorption of water, (B) APTES conjugation, (C) biotinylation, and (D) streptavidin immobilization.

Gaussian oscillator was fit to representative films. The refractive index at 300 nm for the organic layer was $N = 1.558 + I \times 2.3 \times 10^{-7}$ while that used for the protein was $N = 1.591 + I \times 0.024$. For each SiC sample, a minimum of three different locations were measured to gain the average and the population standard deviation of the thickness. When fitting for the thicknesses of subsequent layers, the average thickness of the preceding layer was utilized.

2.2. Fluorescence microscopy

Fluorescence microscopy was performed using a Leica DMRX fluorescence microscope. A filter cube with an excitation of 515–560 nm was used for the streptavidin conjugated samples since the streptavidin-cy3 conjugate protein utilized throughout this work exhibits an excitation at a wavelength of 552 nm. The binding of BSA to the biotinylated SiC samples was investigated using a filter cube with an excitation of 440–480 nm since the FITC labeled BSA used in this work exhibits an excitation at a wavelength of 494 nm. Images were captured with a digital color camera and recorded using the Scion Image program. Recorded images were converted into digitalized intensities using the NIH ImageJ program and subtracted from a background measurement of a biotinylated SiC sample that was not reacted with streptavidin or BSA. For each streptavidin or BSA functionalized sample, a minimum of two images were recorded in order to obtain the averages of the fluorescence intensities.

2.3. AFM

The surface topography of the as-is and functionalized SiC samples was investigated under laboratory ambient conditions with a commercial atomic force microscope (MultiMode Bruker AFM with a Nanoscope V controller, Santa Barbara, CA, USA) in intermittent contact. All AFM images presented in this paper were acquired on an area of 1 μm × 1 μm.

2.4. XPS

SiC oxidation was analyzed using a double-pass cylindrical mirror analyzer XPS instrument with an Al Kα X-ray source and a probing depth of 1.5–6.0 nm depending on the kinetic energy of the photoelectron. Instrument details are described by Schreifels et al. [27]. Relative atomic concentrations were determined using the AugerScan program by subtracting a Shirley-type background and subsequently integrating the area under the remaining peak and dividing by the relative sensitivity. The sensitivity factors were provided by the manufacturer (Kratos sensitivity factors) and are as follows: O 1s = 0.780, C 1s = 0.278, N 1s = 0.477, and Si 2p = 0.328. APTES functionalized SiC samples, biotinylated samples, and streptavidin immobilized samples were analyzed in a Kratos Analytical (Chestnut Ridge, NY, USA) Axis Ultra DLD XPS instrument with a monochromated Al Kα X-ray source at 150 W. X-rays were collected at a 0° angle from surface normal on an area of 300 μm × 700 μm. Instrument details can be found elsewhere [28]. Low resolution survey scans (160 eV pass energy, 0.5 eV step size) and high resolution narrow scans (40 eV pass energy, 0.1 eV step size) of O 1s, N 1s, C 1s, Si 2p3, and S 2s[3] were obtained. To account for minor charging observed in all the XPS measurements, binding energy corrections were made by referencing spectra to the carbon in SiC to 282.5 eV. The CasaXPS program was utilized to analyze the spectra. Because of the potential degradation of the organic

---

[3] The S 2s peak was used for detection due to the S 2p peak overlapping with the Si energy loss peak.
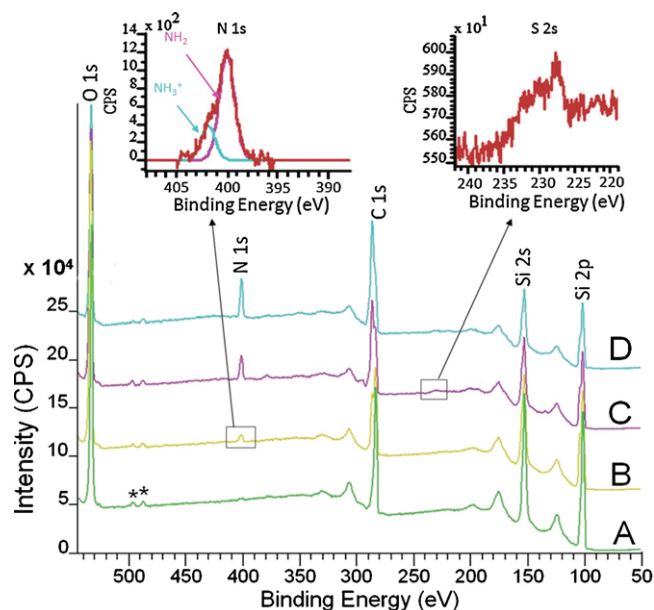
Fig. 1. XPS spectra of (A)–(D) functionalization steps (Scheme 1 from Section 2): (A) SiC after RCA and oxygen plasma cleaning and air exposure, (B) 5 min APTES functionalized SiC, (C) biotinylated SiC, and (D) fully functionalized SiC (oxide, APTES, biotin, and streptavidin). The upper-left inset shows the N 1s peaks from APTES after step (B). The upper-right inset shows the S 2s peak from biotin, which confirms the successful step (C) surface biotinylation. Note: two small peaks marked with * were tentatively assigned to Sn 3d5; the source of contamination of the SiC surface with Sn could not be verified.

layers during X-ray exposure, XPS was either the last or only analysis technique performed on a sample.

2.5. Contact angle

Contact angle measurements were obtained with a static sessile drop method by dispensing 10 μL of deionized water onto the sample surface. At least three contact angle values per sample were obtained to assess averages and population standard deviations.

3. Results and discussion

3.1. SiC surface cleaning (Scheme 1, step A)

XPS, contact angle, ellipsometry, and AFM analyses were performed on the SiC surface post RCA cleaning, oxygen plasma treatment, and air exposure. Following the RCA cleaning procedure, an XPS survey scan and Si, C, and O narrow scans were obtained. The survey scan indicated a surface composition of 10.7% oxygen, 47.9% carbon, and 41.4% silicon (spectra are not shown). The presence of oxygen can be explained by hydroxyl termination of the SiC surface after the RCA cleaning [29], while a high carbon concentration (with larger than the expected C:Si 1:1 ratio) was due to inevitable hydrocarbon contamination during post-RCA air exposure [30]. The hydrocarbon contamination is also visible on the carbon narrow scan as a peak centered at a binding energy of 286.2 eV (not shown).

The XPS survey scan post-RCA, oxygen plasma cleaning, and exposure to air indicated a surface composition of 40.9% oxygen, 25.7% carbon, and 33.3% silicon (see Fig. 1(A)). The significant excess surface oxygen is consistent with reports that oxygen plasma treatment of SiC forms a SiO_2 layer [31]. The presence of SiO_2 is further supported by the silicon narrow scan that exhibits a peak at 101.6 eV for SiC and a second peak at 103.6 eV [29]. Ellipsometry measurements following oxygen plasma treatment indicated an average oxide thickness of 2.6 nm ± 0.2 nm.
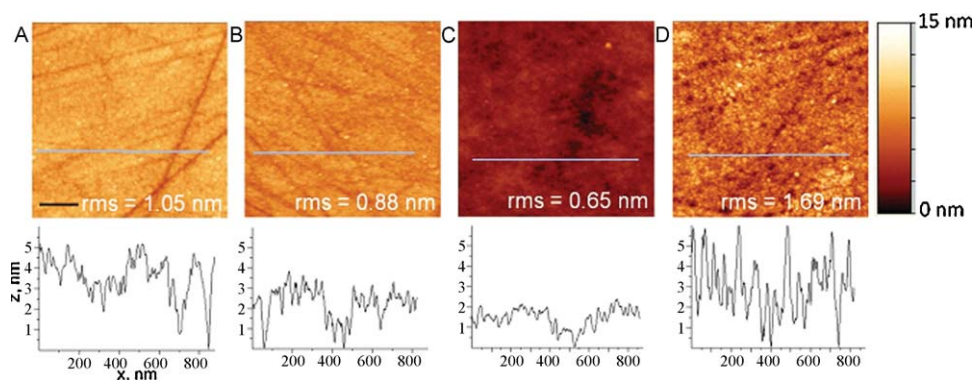
Fig. 2. AFM images with corresponding line scans of (A) RCA cleaned, oxygen plasma cleaned, and air exposed SiC, (B) 5 min APTES functionalized SiC, (C) 16 h APTES functionalized SiC, (D) fully functionalized SiC (oxide, 5 min APTES, biotin, and streptavidin). Scratches from polishing on as-received samples became less pronounced upon (B)–(D) functionalization steps. The 200 nm scale bar in the lower left corner in (A) applies to all 4 images. The vertical bar on the far right is the color-coded *z*-scale. The line scans are taken along the horizontal gray lines shown on the AFM scans. (For interpretation of the references to color in this figure legend, the reader is referred to the web version of the article.)

Contact angle measurements after RCA cleaning, oxygen plasma treatment, and air exposure produced a water contact angle of $6 \pm 2°$ indicating a high hydrophilicity of the oxidized SiC surface. This low contact angle value is consistent with the previously reported near 0° angles for a silanol-terminated SiC surface [13]. Thus, oxygen plasma cleaning can effectively oxidize SiC surfaces and lead to the formation of surface silanol groups upon air exposure. This hydrated SiO_2 layer is necessary for APTES hydrolysis and condensation on the SiC surface [23,29].

The corresponding AFM image of the SiC surface after RCA, oxygen plasma cleaning, and air exposure is shown in Fig. 2(A). The as-received SiC wafer had a relatively rough surface with ≈5–15 nm deep polishing scratches (see Fig. 2(A)) and an average rms roughness value of $1.05 \text{ nm} \pm 0.10 \text{ nm}$. In spite of the rough surface, formation of silicon oxide induced by the oxygen plasma treatment was quite uniform in composition and thickness: the XPS, ellipsometry, and contact angle measurements on at least 3 random spots on the sample surface yielded similar experimental results. The homogeneous oxidation of the SiC surface is required for the formation of a uniform APTES layer.

3.2. APTES functionalization (Scheme 1, step B)

APTES polymerization can often lead to irreproducible layer characteristics [22]. Therefore, optimization of the APTES layer is critical. We have assessed how the APTES solution exposure duration affects the APTES layer thickness. Ellipsometry measurements were obtained for the silanol-terminated SiC samples following 5 min, 1 h, and 16 h immersion in APTES (see Table 1). Given that a dense monolayer of upright APTES should have a thickness of about 0.80 nm based on molecular mechanics calculations [32] (in agreement with the value from [23]), the ellipsometry data revealed that 5 min, 1 h, and 16 h exposures produced layers with thicknesses equivalent to about 1.7, 6.5, and 17 monolayers of APTES, respectively. The increase in thickness with time is likely due to polymerization of APTES molecules with increased deposition time, similar to the observed APTES polymerization on Si substrates [22,23]. APTES agglomeration was found to be uncontrollable and inhomogeneous, as indicated by the large population standard deviations of the layer thicknesses for the 1 h and 16 h treated samples. Successful APTES conjugation was confirmed by water contact angle measurements. Table 1 shows a significant contact angle increase on the processed samples due to the hydrophobic nature of aliphatic chains in APTES, as compared to the plasma cleaned surfaces. Similar wetting behavior has been observed on APTES functionalized Si [23].

AFM results from the APTES functionalized samples are presented in Table 1 and in Fig. 2(B and C). They indicate that the oxidized SiC samples undergo an increasing change in surface morphology following increased APTES deposition times. The rms values decreased significantly following 16 h APTES functionalization revealing a smoothening of the SiC surface to the point of complete disappearance of the polishing scratches (Fig. 2(C)).

XPS analysis confirmed successful immobilization of APTES through the detection of an N 1s nitrogen peak near 400 eV (see Fig. 1, spectrum B for 5 min treated sample). The inset in Fig. 1 shows that this asymmetric peak can be de-convoluted into a 400.2 eV and 401.8 eV peak, which correspond to the neutral (NH_2) and protonated (NH_3^+) forms of the terminal amino group of APTES, respectively [1,22,33,34]. As expected, the N 1s peak scaled up with the APTES exposure time due to the increasing thickness of the APTES layer (quantitative results are summarized in Table 1).

3.3. Biotinylation and streptavidin immobilization (Scheme 1, steps C and D)

The APTES functionalized samples were exposed to the biotin and streptavidin solutions and analyzed with ellipsometry, contact angle, AFM, and XPS. The ellipsometric additive thicknesses of the respective layers are presented in Fig. 3 and in Table S1 in the Supporting Information.

The ellipsometric thicknesses of the biotin layer on the 5 min, 1 h, and 16 h APTES functionalized samples were determined to be $1.6 \text{ nm} \pm 0.4 \text{ nm}$, $3.8 \text{ nm} \pm 2.0 \text{ nm}$, and $16 \text{ nm} \pm 11 \text{ nm}$, respectively (note that the population standard deviations associated with the layer thicknesses are not included in Fig. 3 to avoid data
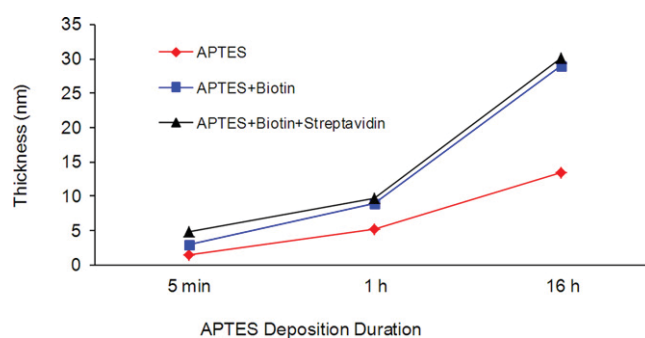
Fig. 3. Ellipsometry thickness of the APTES, APTES and biotin, and APTES, biotin, and streptavidin layers on SiC as a function of APTES deposition duration.

Table 1
Summary of APTES functionalized SiC surface quality in terms of film thickness (ellipsometry), wettability (contact angle), roughness (AFM), and nitrogen content (XPS).

Deposition duration	Thickness (nm)	Contact angle ($\pm 2°$)	AFM image/rms (nm)		Nitrogen (at.%)
0 min (non-functionalized)	n/a	6	Fig. 2(A)	1.05	0
5 min	1.4 ± 0.3	43	Fig. 2(B)	0.88	2.9
1 h	5.2 ± 1.8	59	Not shown	1.00	Not analyzed
16 h	$13. \pm 5.$	68	Fig. 2(C)	0.65	9.9

crowding). Significant scaling up of the biotin thickness with the APTES thickness is likely due to the fact that biotin, as a small molecule, is able to access both external and internal amino groups in polymerized APTES, leading to uncontrollable accumulation of biotin on thick, i.e., the 1 h and 16 h exposed, APTES layers. The large population standard deviations of the biotin thicknesses on both of these two samples, unlike for the 5 min APTES exposed sample, indicate significant non-uniformity of the biotin layers. Consequently, the inhomogeneous biotin build up on polymerized APTES led to complications in quantitation of subsequent streptavidin binding. Upon exposure to streptavidin, the 1 h and 16 h APTES functionalized and biotinylated samples resulted in a 0.7 nm $\pm$ 0.6 nm and a 1.0 $\pm$ 1.5 nm thick streptavidin layer (Fig. 3), respectively.

Given such large uncertainties, the attachment of streptavidin to these two samples was statistically insignificant. The non-uniform, non-reproducible biotin layers and the statistically insignificant streptavidin accumulation on the 1 h and 16 h APTES functionalized samples establish the critical role of the APTES layer in subsequent behavior and indicate only near monolayer films should be utilized for reproducible biotinylation and streptavidin immobilization.

The ellipsometric thickness of the biotin layer formed on the 5 min APTES functionalized samples of 1.6 nm $\pm$ 0.4 nm (Fig. 3 and Table S1) nominally corresponds to 1.5 monolayers of biotin based on the 1.1 nm height of the molecular fragment that binds to APTES [32]. The experimental biotin layer thickness suggests that nearly all (1.7 layers as stated above) of the APTES on the SiC surface is available for binding, consistent with the behavior of the thicker, polymeric APTES layers.

The water contact angle decreased by 7° to a value of 36 $\pm$ 2° following biotinylation (Table S2). This decrease in contact angle, as compared to the APTES functionalized samples, can be attributed to the polar ureido- and tetrahydrothiophene-rings of biotin. The ureido- and tetrahydrothiophene-rings of biotin are more hydrophilic than APTES and therefore, the contact angle of the biotinylated samples is less than that of the APTES functionalized samples. For comparison, a thiolated biotin on gold surface demonstrated water contact angles of 33° [35], in good agreement with our results for biotinylated SiC.

The XPS survey scan of a biotinylated SiC sample is shown in Fig. 1(C). The nitrogen signal for the biotin/APTES bi-layer is more intense than the nitrogen signal for the APTES only layer (Fig. 1(B)). The nitrogen signal for the biotin/APTES bi-layer does increase the expected three-fold as compared to the APTES only layer due to the two nitrogen atoms per biotin molecule. A sulfur 2 s peak centered around a binding energy of 227.7 eV appears on the XPS spectrum following biotinylation (see right inset of Fig. 1). The sulfur peak can be attributed to the sulfur atom contained within the tetrahydrothiophene-ring of biotin, since up to this functionalization step, no chemicals employed in this work contained sulfur atoms. The XPS sulfur peak provides further proof that biotin is bound to the APTES functionalized SiC surface.

The ellipsometric thickness of the streptavidin layer formed on the biotinylated and 5 min APTES functionalized SiC samples was measured to be 1.8 $\pm$ 0.3 nm (Fig. 3 and Table S1). The molecular dimensions of streptavidin are 4.2 nm × 4.2 nm × 5.6 nm [36], suggesting that a sub-monolayer of streptavidin was

immobilized on the biotinylated samples. This is consistent with previous experimental results for a similar biotin/streptavidin pair, which attributed incomplete protein surface coverage to steric hindrance that prevented the immobilization of streptavidin molecules directly next to one another [37].

The AFM image of streptavidin functionalized SiC (Fig. 2(D)) appears granular and there are small spheres or circular dots spread all over the SiC surface. These spheres are likely streptavidin molecules immobilized on the SiC surface. Furthermore, the AFM data indicates that the spheres have an approximate height of 4.5 nm, close to the expected height of streptavidin [36]. The rms roughness value increased post streptavidin immobilization which is in agreement with the ellipsometry measurements. A 1.8 nm thick, sub-monolayer of streptavidin on the SiC surface indicates non-uniform streptavidin binding which would result in a roughening of the functionalized SiC surface.

The water contact angle of the streptavidin immobilized SiC samples was determined to be 33° $\pm$ 2° (Table S2) indicating a slight decrease in the contact angle following streptavidin conjugation to SiC. Almost all proteins have a hydrophilic exterior, permitting solubility in water and yielding a relatively low water contact angle. This is likely the reason for the decreased water contact angle on the streptavidin functionalized samples. A water contact angle of 24.3° has been reported for streptavidin on glass [36].

Fig. 1(D) shows the XPS survey scan of a streptavidin functionalized SiC sample. The survey scan reveals an intense N 1s signal, which can be attributed to the many amide or peptide linkages found in the protein. The N 1s signal from the streptavidin functionalized SiC sample (Fig. 1(D)) is obviously larger than that from the biotinylated SiC sample (Fig. 1(C)) due to a higher density of N atoms in the streptavidin/biotin bi-layer. Also, the S 2s signal that appeared following biotinylation is weaker after streptavidin immobilization due to possible shielding of the sulfur atoms by the streptavidin top layer. Thus, the XPS data is a good indication that streptavidin is indeed immobilized on the biotinylated SiC surface.

The immobilization of streptavidin on the biotinylated SiC samples was confirmed using fluorescence microscopy. Fig. 4(C) illustrates the uniform bright-red fluorescence from the cy3-labeled streptavidin functionalized sample. Therefore, it can be concluded that there was successful attachment of streptavidin to the biotinylated SiC surface with each functionalization step being validated using a suite of characterization methods: ellipsometry, XPS, contact angle, AFM, and fluorescence microscopy.

3.4. Specificity and selectivity of streptavidin binding

Biosensors rely on the signal transduction associated with the selective recognition of a biological species of interest [38]. Thus, if the biotinylated SiC samples are to be employed as a biosensing platform, it is imperative that only the analyte of interest, i.e. streptavidin, has the ability to be specifically conjugated to the biotinylated SiC surface. To test the selectivity of the biotinylated SiC samples, they were exposed to BSA, a serum protein that has no affinity for biotin [3].

Prior to this test, the ability of streptavidin and BSA to bind to bare and to APTES functionalized SiC surfaces was also examined to assess non-specific protein binding. Starting with the bare,
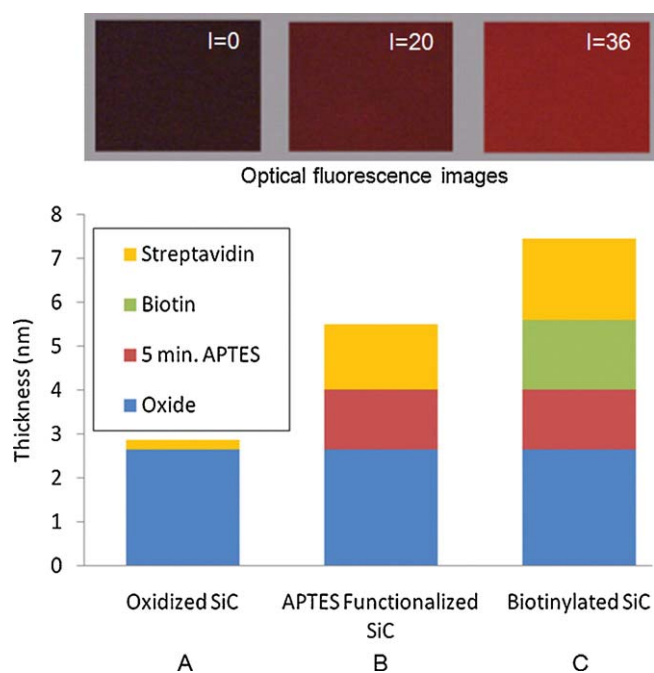
Fig. 4. Ellipsometry thicknesses for streptavidin immobilization on: (A) oxidized SiC, (B) APTES functionalized SiC, and (C) biotinylated SiC. Corresponding fluorescence microscopy images after protein exposure (magnification 10×) are shown in the gray frame above each thickness bar with the integrated fluorescence intensity values in the upper-right corner.

silanol-terminated (Scheme 1, step A) surface, exposure to proteins for 2 h, both streptavidin and BSA, showed an insignificant surface attachment with the ellipsometric layer thicknesses of 0.2 ± 0.02 nm and 0.5 ± 0.02 nm, respectively (Table 2). On the contrary, 5 min APTES functionalized (Scheme 1, step B) samples produced a noticeable build-up of streptavidin and BSA upon 2 h exposure to the respective proteins with thicknesses of 1.5 ± 0.2 nm and 1.2 ± 0.02 nm, respectively (Table 2). The streptavidin layer thickness and corresponding fluorescence response on "step A" and "step B" processed samples are summarized in Fig. 4(A and B) (results for BSA are not included). Therefore, there was significant non-specific binding of streptavidin and BSA to the APTES functionalized surface. It is known that BSA does not adsorb onto negatively charged silica surfaces at pH $\approx$7 [39]. At a pH of less than 8, the amino group of APTES can be protonated, while streptavidin and BSA carry a negative charge at pH values above their isoelectric points [16,40]. Since a pH of 7.4 was utilized in this study, streptavidin and BSA molecules were likely electrostatically bound to the APTES layer on the SiC surface.

The issue of non-specific protein attachment was also examined on fully processed SiC surfaces. After 2 h protein exposure to biotinylated (Scheme 1, step C) surfaces, the ellipsometric thickness of the streptavidin layer was measured to be 1.8 nm $\pm$ 0.3 nm, while the BSA layer thickness on the biotinylated SiC samples was measured as a negative value, -0.4 ± 0.2 nm (Table 2).

Table 2
Summary of streptavidin and BSA layer thicknesses (ellipsometry) on treated SiC surfaces.

	Streptavidin thickness (nm)	BSA thickness (nm)
Clean SiC (post RCA, oxygen plasma, and air exposure)	0.2 ± 0.02	0.5 ± 0.02
5 min APTES functionalized SiC	1.5 ± 0.2	1.2 ± 0.02
5 min APTES functionalized and biotinylated SiC	1.8 ± 0.3	-0.4 ± 0.2

Fluorescence imaging confirmed the results with bright red fluorescence of streptavidin on streptavidin conjugated samples (Fig. 4(C)) and the absence of green fluorescence of BSA on BSA treated surfaces (not shown). The inability of BSA to bind to the biotinylated SiC surface reveals that the fully processed samples (steps A through C in Scheme 1) are indeed selective to streptavidin. In addition, Fig. 4(B and C) illustrates that the specifically attached streptavidin layer is significantly more fluorescent than the non-specifically bound layer.

Noteworthy, non-specific electrostatic binding of streptavidin and BSA to APTES reveals the importance of step C (biotinylation) in Scheme 1; the SiC surface must be uniformly biotinylated before proceeding with streptavidin immobilization in order to limit non-specific protein attachment to APTES. Functionalization protocols for biosensor development must eliminate non-specific interactions.

Finally, the ability of FBS (in which four biotin molecules per each streptavidin molecule are presumed to "saturate" all specific binding sites in the protein), to react with the APTES and biotin functionalized SiC surface was tested. The FBS thickness on the APTES functionalized surface was measured to be 2.8 ± 0.02 nm due to the electrostatic binding of negatively charged FBS to the positively charged APTES functionalized surface. This result agrees well with the non-specific binding of streptavidin alone on APTES as discussed above. There was more limited, 0.2 ± 0.02 nm thick, non-specifically bound FBS on the biotinylated surface, which confirms that the predominant mode of streptavidin binding to biotinylated surfaces is specific. The utility of using APTES functionalization to specifically attach biomolecules to SiC surfaces is thus demonstrated.

4. Conclusions

AFM, XPS, ellipsometry, and contact angle measurements were utilized to develop and validate the optimum conditions for the specific attachment of streptavidin to the (0 0 0 1) SiC surface. This work demonstrated that the first-step uniform oxidation of the SiC surface enables its successful APTES functionalization. RCA and oxygen plasma treatment produced a homogeneous surface oxide layer, which upon exposure to air, transformed into a silanol-terminated surface that facilitated APTES immobilization. The covalent attachment of APTES to the oxidized/silanol-terminated SiC surface was observed and it was determined that the structure, thickness, wettability, and reactivity of the APTES films is dependent on deposition time. A 5 min deposition time produces an APTES layer that resembles an ordered self-assembled monolayer and permits controllable biotinylation and streptavidin immobilization. It was shown that a dense, functional layer of biotin was formed on the 5 min APTES functionalized surface demonstrated by successful streptavidin conjugation. Streptavidin molecules formed a sub-monolayer, likely due to steric hindrance, on the close-packed biotinylated and APTES functionalized SiC surface. The binding of streptavidin directly to the silanol-terminated SiC surface and to the 5 min APTES functionalized SiC surface was investigated and it was shown that there was little non-specific binding of streptavidin to oxidized SiC. There was however, significant non-specific, electrostatic binding of streptavidin to the APTES functionalized SiC surface. Therefore, it is of utmost importance to uniformly and fully biotinylate the SiC surface to prevent the non-specific attachment of streptavidin to APTES. In addition, the selectivity of biotinylated SiC samples for the streptavidin protein was demonstrated. Ellipsometry and fluorescence microscopy revealed no significant binding of the BSA protein to the biotinylated SiC surface. The APTES functionalized and biotinylated SiC surface shows promise as a potential biosensing platform for the

selective attachment and detection of streptavidin and other protein molecules.

Acknowledgment

The authors acknowledge with gratitude the financial support of the National Science Foundation (Grant # ECCS-0901712).

Appendix A. Supplementary data

Supplementary data associated with this article can be found, in the online version, at doi:10.1016/j.apsusc.2012.02.137.

References

[1] A. Arranz, D. Palacio, D. Garcia-Fresnadillo, G. Orellana, A. Navarro, E. Munoz, Influence of surface hydroxylation on 3-aminopropyltriethoxysilane growth mode during chemical functionalization of GaN surfaces: an angle-resolved X-ray photoelectron study, Langmuir 24 (16) (2008) 8667–8671.

[2] R. Yakimova, G. Steinhoff, R.M. Petoral, C. Vahlberg, V. Khranovskyy, G.R. Yazdi, K. Uvdal, A.L. Spetz, Novel material concepts of transducers for chemical and biosensors, Biosens. Bioelectron. 22 (12) (2007) 2780–2785.

[3] B.S. Kang, F. Ren, L. Wang, C. Lofton, W.W. Tan, S.J. Pearton, A. Dabiran, A. Osinsky, P.P. Chow, Electrical detection of immobilized proteins with ungated AlGaN/GaN high-electron-mobility transistors, Appl. Phys. Lett. 87 (2005) 023508-1–023508-3.

[4] F. Patolsky, G. Zheng, C.M. Lieber, Fabrication of silicon nanowire devices for ultrasensitive, label-free, real-time detection of biological and chemical species, Nat. Protoc. 1 (4) (2006) 1711–1724.

[5] E. Stern, A. Vacic, M.A. Reed, Semiconducting nanowire field-effect transistor biomolecular sensors, IEEE Trans. Electron. Dev. 55 (11) (2008) 3119–3130.

[6] N. Chaniotakis, N. Sofikiti, Novel semiconductor materials for the development of chemical sensors and biosensors: a review, Anal. Chim. Acta 615 (2008) 1–9.

[7] R. Yakimova, R.M. Petoral, G.R. Yazdi, C. Vahlberg, A.L. Spetz, K. Uvdal, Surface functionalization and biomedical applications based on SiC, J. Phys. D: Appl. Phys. 40 (2007) 6435–6442.

[8] S. Santavirta, M. Takagi, L. Nordsletten, A. Anttila, R. Lappalainen, Y.T. Konttinen, Biocompatibility of silicon carbide in colony formation test in vitro: a promising new ceramic THR implant coating material, Arch. Orthop. Traum Surg. 118 (1–2) (1998) 89–91.

[9] C. Coletti, M.J. Jaroszeski, A. Pallaoro, A.M. Hoff, S. Iannotta, S.E. Saddow, Biocompatibility and wettability of crystalline SiC and Si surfaces, in: Proceedings of the 29th Annual International Conference of the IEEE EMBS, 2007, pp. 5849–5852.

[10] J.B. Casady, R.W. Johnson, Status of silicon carbide (SiC) as a wide-bandgap semiconductor for high-temperature applications: a review, Solid-State Electron. 39 (10) (1996) 1409–1422.

[11] K. Rottner, M. Frischholz, T. Myrtveit, D. Mou, K. Nordgen, A. Henry, C. Hallin, U. Gustafsson, A. Schoner, SiC power devices for high voltage applications, Mater. Sci. Eng. B 61–62 (1999) 330–338.

[12] G.T. Hermanson, Bioconjugate Techniques, 2nd ed., Academic Press, San Diego, CA, USA, 2008.

[13] M. Rosso, A. Arafat, K. Schroen, M. Giesbers, C.S. Roper, R. Maboudian, H. Zuilhof, Covalent attachment of organic monolayers to silicon carbide surfaces, Langmuir 24 (2008) 4007–4012.

[14] B. Baur, G. Steinhoff, J. Hernado, O. Purrucker, M. Tanaka, B. Nickel, M. Stutzmann, M. Eickhoff, Chemical functionalization of GaN and AlN surfaces, Appl. Phys. Lett. 87 (2005) 263901–263903.

[15] N.A. Lapin, J.Y. Chabal, Infrared characterization of biotinylated silicon oxide surfaces, surface stability, and specific attachment of streptavidin, J. Phys. Chem. B 113 (2009) 8776–8783.

[16] S. Sivasankar, S. Subramaniam, D. Leckband, Direct molecular level measurements of the electrostatic properties of a protein surface, Proc. Natl. Acad. Sci. U.S.A. 95 (1998) 12961–12966.

[17] J.F. Mooney, A.J. Hunt, J.R. McIntosh, C.A. Liberko, D.M. Walba, C.T. Rogers, Patterning of functional antibodies and other proteins by photolithography of silane monolayers, Proc. Natl. Acad. Sci. U.S.A. 93 (1996) 12287–12291.

[18] D. Moll, C. Huber, C. Schlegel, D. Pum, U.B. Sleytr, M. Sàra, S-layer-streptavidin fusion proteins as template for nanopatterned molecular arrays, Proc. Natl. Acad. Sci. U.S.A. 99 (23) (2002) 14646–14651.

[19] N.K. Chaki, K. Vijayamohanan, Self-assembled monolayers as a tunable platform for biosensor applications, Biosens. Bioelectron. 17 (1–2) (2002) 1–12.

[20] K.A. Reinhardt, W. Kern, Handbook of Semiconductor Wafer Cleaning Technology, 2nd ed., William Andrew Publishing, New Jersey, USA, 2008.

[21] K.H. Choi, J.P. Bourgoin, S. Auvray, D. Esteve, G.S. Duesberg, S. Roth, M. Burghard, Controlled deposition of carbon nanotubes on a patterned substrate, Surf. Sci. 462 (1–3) (2000) 195–202.

[22] J. Kim, P. Seidler, C. Fill, L.S. Wan, Investigations of the effect of curing conditions on the structure and stability of amino-functionalized organic films on silicon substrates by Fourier transform infrared spectroscopy, ellipsometry, and fluorescence microscopy, Surf. Sci. 602 (21) (2008) 3323–3330.

[23] J.A. Howarter, J.P. Youngblood, Optimization of silica silanization by 3-aminopropyltriethoxysilane, Langmuir 22 (26) (2006) 11142–11147.

[24] D.E. Aspnes, Approximate solution of ellipsometric equations for optically biaxial crystals, J. Opt. Soc. Am. 70 (10) (1980) 1275–1277.

[25] S. Zollner, J.G. Chen, E. Duda, T. Wetteroth, S.R. Wilson, J.N. Hilfiker, Dielectric functions of bulk 4H and 6H SiC and spectroscopic ellipsometry studies of thin SiC films on Si, J. Appl. Phys. 85 (1999) 8353–8362.

[26] I.H. Malitson, Interspecimen comparison of the refractive index of fused silica, J. Opt. Soc. Am. 55 (1965) 1205–1208.

[27] J.A. Schreifels, N.H. Turner, R.E. Morris, A comparison of x-ray photoelectron spectroscopy and auger electron spectroscopy depth profiles for magnesium implants, Surf. Sci. 84 (1) (1995) 23–29.

[28] F.W. DelRio, K.L. Steffens, C. Jaye, D.A. Fischer, R.F. Cook, Elastic, adhesive, and charge transport properties of a metal–molecule–metal junction: the role of molecular orientation, order, and coverage, Langmuir 26 (3) (2010) 1688–1699.

[29] S. Dhar, O. Seitz, M.D. Halls, S. Choi, Y.J. Chabal, L.C. Feldman, Chemical properties of oxidized silicon carbide surfaces upon etching in hydrofluoric acid, J. Am. Chem. Soc. 131 (46) (2009) 16808–16813.

[30] S. Dhar, Y.W. Song, L.C. Feldman, T. Isaacs-Smith, C.C. Tin, J.R. Williams, G. Chung, T. Nishimura, D. Starodub, T. Gustafsson, E. Garfunkel, Effect of nitric oxide annealing on the interface trap density near the conduction bandedge of 4H–SiC at the oxide/(112$\bar{0}$) 4H–SiC interface, Appl. Phys. Lett. 84 (9) (2004) 1498–1500.

[31] C. Önneby, C.G. Pantano, Silicon oxycarbide formation on SiC surfaces and at the SiC/SiO$_2$ interface, J. Vac. Sci. Technol. A 15 (3) (1997) 1597–1602.

[32] CrystalMaker, Version 2.3, Software for Technical Computation, CrystalMaker Software Ltd., Oxfordshire, UK, 2011.

[33] C. Chu-jiang, S. Zhi-gang, X. Yu-shan, M. Shu-lin, Surface topography and character of γ-aminopropyltriethoxysilane and dodecyltrimethoxysilane films adsorbed on the silicon dioxide substrate via vapour phase deposition, J. Phys. D: Appl. Phys. 39 (22) (2006) 4829–4837.

[34] J. Kim, P. Seidler, L.S. Wan, C. Fill, Formation, structure, and reactivity of amino-terminated organic films on silicon substrates, J. Colloid Interface Sci. 329 (1) (2009) 114–119.

[35] V.H. Perez-Luna, M.J. O'Brien, K.A. Opperman, P.D. Hampton, G.P. Lopez, L.A. Klumb, P.S. Stayton, Molecular recognition between genetically engineering streptavidin and surface-bound biotin, J. Am. Chem. Soc. 121 (27) (1999) 6469–6478.

[36] C.J. vanOss, R.F. Giese, P.M. Bronson, A. Docoslis, P. Edwards, W.T. Ruyechan, Macroscopic-scale surface properties of streptavidin and their influence on aspecific interactions between streptavidin and dissolved biopolymers, Colloids Surf. B 30 (1–2) (2003) 25–36.

[37] J. Spinke, M. Liley, F.-J. Schmitt, H.-J. Guder, L. Angermaier, W. Knoll, Molecular recognition at self-assembled monolayers: optimization of surface functionalization, J. Chem. Phys. 99 (9) (1993) 7012–7019.

[38] F. Patolsky, C.M. Lieber, Nanowire nanosensors, Mater. Today 8 (4) (2005) 20–28.

[39] F.J. MacRitchie, The adsorption of proteins at the solid/liquid interface, J. Colloid Interface Sci. 38 (2) (1972) 484–488.

[40] C.B. Anfinsen, J.T. Edsall, F.M. Richards, Advances in Protein Chemistry, vol. 31, Academic Press, San Diego, CA, USA, 1991.